Research Square

Preprints are preliminary reports that have not undergone peer review.
They should not be considered conclusive, used to inform clinical practice,
or referenced by the media as validated information.

Bioinspired Synthesis of Glycinoeclepin A Enables Chemical Interrogation of Its Plausible Biogenesis

Jun Deng

deng.jun@nankai.edu.cn

State Key Laboratory and Institute of Elemento-Organic Chemistry, Frontiers Science Center for New Organic Matter, College of Chemistry, Nankai University https://orcid.org/0000-0002-7463-1329

Xianwen Long

State key laboratory and Institute of Elemento-Organic Chemistry, Nankai University, China

Zhilong Feng

State Key Laboratory and Institute of Elemento-Organic Chemistry, Frontiers Science Center for New Organic Matter, College of Chemistry, Nankai University

Yaqiu Zhao

State Key Laboratory for Quality Ensurance and Sustainable Use of Dao-di Herbs, National Resource Center for Chinese Materia Medica, China Academy of Chinese Medical Sciences (CACMS), Beijing, China

Tao Zhang

State Key Laboratory and Institute of Elemento-Organic Chemistry, Frontiers Science Center for New Organic Matter, College of Chemistry, Nankai University

Jie Chen

State Key Laboratory and Institute of Elemento-Organic Chemistry, Frontiers Science Center for New Organic Matter, College of Chemistry, Nankai University

Jun Li

State Key Laboratory and Institute of Elemento-Organic Chemistry, Frontiers Science Center for New Organic Matter, College of Chemistry, Nankai University

Huimin Huang

State Key Laboratory and Institute of Elemento-Organic Chemistry, Frontiers Science Center for New Organic Matter, College of Chemistry, Nankai University

Luqi Huang

National Resource Centre for Chinese Materia Medica, China Academy of Chinese Medical Sciences https://orcid.org/0000-0002-2070-4318

Luhua Wang

State Key Laboratory and Institute of Elemento-Organic Chemistry, Frontiers Science Center for New Organic Matter, College of Chemistry, Nankai University

Article

Keywords:

Posted Date: June 4th, 2026

DOI: https://doi.org/10.21203/rs.3.rs-9860163/v1

License: This work is licensed under a Creative Commons Attribution 4.0 International License.
Read Full License

Additional Declarations: There is **NO** Competing Interest.

Bioinspired Synthesis of Glycinoeclepin A Enables Chemical Interrogation of Its Plausible Biogenesis

Xianwen Long,[1,3] Zhilong Feng,[1,3] Yaqiu Zhao,[2,3] Tao Zhang,[1] Jie Chen,[1] Jun Li,[1] Huimin Huang,[1] Luhua Wang,[1] Luqi Huang,*[,2] Jun Deng*[,1]

This paper is dedicated to Prof. E. J. Corey for his pioneering work in natural product synthesis.

[1]State Key Laboratory and Institute of Elemento-Organic Chemistry, Frontiers Science Center for New Organic Matter, College of Chemistry, Nankai University, Tianjin 300071, China，E-mail: dengjun@nankai.edu.cn

[2]State Key Laboratory for Quality Ensurance and Sustainable Use of Dao-di Herbs, National Resource Center for Chinese Materia Medica, China Academy of Chinese Medical Sciences, Beijng, 100700, P. R. China

Abstract: A bioinspired synthesis of glycinoeclepin A—the most potent hatching stimulus for the soybean cyst nematode—has been achieved from commercially available γ-oryzanol. The route features three key transformations: TFDO-directed sp^3 C–H oxidation coupled with side-chain scission, a programmed skeletal reorganization (dyotropic rearrangement → epoxidation/Meinwald cascade), and a photo-oxidative decarbonylation. Mechanistic studies, including control experiments and comparative reactivity analysis, reveal how solvent and acid modulate competing carbocation pathways, governing the balance between methyl migration and hydride shift processes. This sequence provides a concise and scalable 17-step entry to glycinoeclepin A and advances a testable framework for understanding carbocation-driven skeletal rearrangements in the assembly of eclepin-type biogenesis.

Introduction

As a cornerstone crop, soybean supplies a major share of global plant-based proteins, fats, and oils. However, the soybean cyst nematode (Heterodera glycines) remains the leading constraint on soybean production, responsible for >US$1.5 billion in annual losses in the United States alone.[1-3] Its success stems from a durable life stage: after fertilization, the female's cuticle hardens into a cyst that protects eggs from desiccation and temperature extremes, allowing them to persist in soil for decades without a host (**Scheme 1A**).[4] When a chemical hatching stimulus is present, second-stage juveniles emerge and invade roots; in its absence, the encysted eggs remain dormant. Conventional nematicides have limited access to this hidden egg bank, highlighting the need for complementary, environmentally friendly strategies.[5-7] One such strategy is "suicide hatching": rather than poisoning nematodes, one applies trace amounts of the natural hatching stimulus after harvest, when no soybean hosts are present, forcing juveniles to hatch at the wrong time and die naturally within weeks. Glycinoeclepin A (**1**), a scarce nortriterpenoid isolated in vanishing amounts from legumes, is the most potent hatching stimulus known, active at picomolar levels (1×10^{-11}– 1×10^{-12} g ml^{-1} in water).[8,9] Its extraordinary efficacy and selectivity make it an attractive lead for field deployment and for probing the chemosensory biology of SCN. Yet the compound's natural abundance (~0.4 mg/ton of dried kidney bean roots) severely constrains mechanistic studies, structure–activity relationship exploration, and practical testing.[10]

Chemical synthesis therefore remains the most practical route to glycinoeclepin A (**1**) and its analogues (**Scheme 1B**). To date, five impressive total syntheses have been reported—most notably by Muai[11], Corey[12], Mori[13], Tanino[14], and more recently Hu.[14] These syntheses generally adopt a convergent strategy involving initial construction of the A/B and D/E ring systems, followed by late-stage coupling. Despite these synthetic achievements, the biosynthetic logic underlying glycinoeclepin A (**1**) remains poorly understood. Four years after completing their total synthesis, Corey and co-workers[16] reported a striking biomimetic synthesis of 12-deoxyglycinoeclepin A (**7**) from abietospiran (22 steps, see

Scheme S1 for details), featuring carbon-skeleton rearrangement, selective C6–C7 bond cleavage, and Barton decarboxylation. (**Scheme 1C**). This work stands as a landmark study in bioinspired glycinoeclepin chemistry and provides an influential framework for considering its possible biogenesis. However, three critical challenges remained. First, abietospiran (**2**) has become difficult to obtain, rendering that otherwise elegant strategy impractical and motivating the development of a new entry to site-selective C17 sp^3 C–H oxidation. Second, late-stage, site-selective installation of the C12 hydroxy group within that framework proved difficult in the presence of more reactive C–H sites, despite the importance of this functionality to the biological activity of glycinoeclepin A (**1**). Third, the decarbonylative C-ring fragmentation required to complete the natural product had not been established. In this work, we set out to solve these three problems, thereby realizing a fully developed bioinspired synthesis of glycinoeclepin A (**1**) and, in turn, enabling chemical interrogation of its plausible biogenesis.

Chemical emulation has proven to be a powerful tool for elucidating the biosynthetic logic of complex natural products and guiding the discovery of related molecular architectures, as exemplified by Trauner's synthesis of epicolactone.[17] Although the biosynthetic pathway of glycinoeclepin A remains unresolved,[18] we devised a biosynthetically inspired design based on biosynthetic network analysis (**Scheme 1D**).[19] From cycloartenol (**8**), sequential side-chain oxidation and degradation could plausibly furnish acid **9**. Selective sp^3 C–H oxidation at C17 could then furnish lactone **10**, which could serve as a trigger for the subsequent carbocation-cation initiated skeletal rearrangement. A dytropic rearrangement followed by epoxidation delivers the mono-methyl migration product **11**. Subsequent epoxide opening and a Meinwald rearrangement cascade could furnish alcohol **12**, thereby offering a plausible origin for the C12 hydroxy group. Finally, D-ring oxidation and B-ring oxidative decarbonylation elaborate **12** into glycinoeclepin A (**1**). Although this sequence is not intended as a literal proposal for the enzymatic pathway, it captures the key skeletal logic required to transform a cycloartane precursor into the glycinoeclepin framework.

To evaluate this biosynthetically inspired design, we undertook a bioinspired synthesis of glycinoeclepin A (**1**) with the dual goals of accessing the natural product efficiently and probing the mechanistic basis of its key skeletal rearrangements. The key challenges posed by this route were as follows: 1) Site-selective oxidation at C17 concurrent with strategic C23-C24 bond cleavage; 2) programmed skeletal reorganization to establish the C13 and C17 quaternary stereocenters and stereoselective installation of the C12 hydroxyl group; 3) selective decarbonylation at C6.

Results and Discussion

1) sp^3 C–H oxidation and side-chain scission to lactone 17

Our first objective was to access lactone **17**, a pivotal intermediate whose preparation required oxidative side-chain scission in tandem with site-selective C17 oxidation (**Scheme 3**). Although considerable advances have been made in C–H functionalization, [20-22] site-selective oxidation of unactivated sp^3 C–H bonds in complex frameworks remains challenging. [23-25] In 2022, the Heretsch group and our group independently exploited C17 sp^3 C–H bond oxidation in synthetic studies toward spirochensilide A.[26] The Heretsch group employed a Suárez-type radical–polar crossover strategy to realize C17 sp^3 C–H oxidation and the ensuing methyl migration.[26a] More recently, they extended this strategy to the cycloartenol skeleton.[26c] In contrast, we employed an intramolecular trifluoromethyl-dioxirane (TFDO)-based sp^3 C–H bond oxidation strategy.[26b, 27] Guided by this precedent, we selected the TFDO-based approach here because it offers predictable site selectivity through a six-membered transition-state geometry and can be readily implemented through installation of a trifluoromethyl ketone directing group, which is easily introduced by $TMSCF_3$ addition to the corresponding aldehyde followed by oxidation.[28]

Commercial γ-oryzanol (**14**), an inexpensive precursor to cycloartenol, was used as an approximately 1:1.3 mixture of its two major side-chain isomers.[29] The desired aldehyde **15** was obtained from **14** in three steps through hydrolysis, C3 acetylation, and ozonolysis of the C24–C25 double bond, while by-product **15a** could be recycled to **15** in three

additional steps via Baeyer–Villiger oxidation, ester reduction, and C3 acetylation. Installation of the directing group by $TMSCF_3$ addition, desilylation, and DMP oxidation furnished trifluoromethyl ketone **16**. Consistent with our prior studies on lanosterol derivatives, oxidation of 16 under TFDO-generating conditions (Oxone®/$NaHCO_3$/EDTA·2Na) afforded tertiary alcohol **16a** through site-selective C17 hydroxylation. Intermediate **16a** readily cyclized to the corresponding hemiketal **16b**, either slowly in solution or rapidly in the solid state, reflecting the inherent stability of this six-membered hemiacetal motif. Our initial efforts were directed toward conversion of **16b** into the corresponding six-membered lactone **16c**. Unexpectedly, however, under modified oxidative conditions we observed direct formation of the five-membered lactone **17** in 76% yield.

To elucidate the origin of this unexpected product, a series of control experiments were conducted (see Supporting Information). These studies support a cascade pathway in which **16** first undergoes TFDO-mediated C17 oxidation to give **16a**, followed by α-oxidation under the basic conditions to generate a transient α-hydroxy intermediate. Rapid cyclization then furnishes hemiacetal **16d**, and subsequent Jones oxidation promotes selective C23–C24 diol cleavage together with oxidation of the hemiacetal to deliver lactone **17**. The structure of **17** was unambiguously confirmed by single-crystal X-ray diffraction of its C3-deacetylated derivative. Because the synthetic target at this stage was the five-membered lactone **17**, this unexpected sp^3 C–H oxidation/side-chain scission cascade proved highly advantageous, obviating the need for a separate one-carbon degradation from six-membered lactone **16c**. More broadly, this transformation effectively merges site-selective C–H oxidation with side-chain truncation in a single operation and highlights a previously underexplored mode of oxidative skeletal editing in triterpenoid synthesis.

2) Programmed skeletal reorganization (17 → 20)

With key lactone **17** in hand, we turned to a programmed skeletal reorganization (**Scheme 3**).[20-33] Our initial objective was to promote the first C13 methyl migration while suppressing the subsequent C14 methyl migration and cyclopropane opening. We envisaged that acid activation of lactone **17** would initiate a dyotropic rearrangement,[34] furnishing the C13-methyl-migrated lactone **17b**. From lactone **17b**, two principal reaction pathways can be envisioned. In the desired pathway (path a, red), the rearrangement terminates after the first methyl migration, followed by deprotonation to furnish the mono-migrated products **18a**/**18**. In the competing pathway (path b, blue), a second methyl migration and cyclopropane opening occur to give the more extensively rearranged product **18b**. More generally, lactone-initiated rearrangements of this type can progress beyond the initial migration to more stable allylic carbocation-derived intermediates, ultimately leading to conjugated diene systems after proton elimination.

To control this balance, we systematically examined the effects of acid and solvent on the dyotropic rearrangement (**Table 1**). At 15 °C in DCM, marked selectivity differences were observed: TFA and Et_2AlCl failed to initiate the reaction (**entries 1 and 2**), whereas $FeCl_3$ and BF_3•OEt_2 afforded mixtures of **18a** and **18b** (**entries 3 and 4**). In contrast, $Bi(OTf)_3$ selectively produced **18a** in 60% yield (**entry 5**), whereas $Sc(OTf)_3$ favored the more rearranged product **18b** in 42% yield (**entry 6**). Further optimization increased the yield of **18b** to 60% with $Sc(OTf)_3$ in HFIP at 0 °C (**entry 7**). By contrast, in MeOH at 80 °C, both $Sc(OTf)_3$ and $Bi(OTf)_3$ cleanly furnished the methyl ester **18** in 90% and 81% yield, respectively (**entries 14 and 12**). Other combinations, such as TFA/HFIP at 0 °C and $FeCl_3$/MeOH at 80 °C, led to more complex reaction mixtures, whereas deacetylated **18a** was obtained in 80% yield upon heating in H_2SO_4/dioxane (**entry 11**). Taken together, these data demonstrate that both acid identity and reaction medium exert decisive control over whether the rearrangement terminates after the first migration or proceeds toward the more rearranged diene **18b**. On the basis of these results, a one-pot protocol using $Sc(OTf)_3$/MeOH (80 °C) was selected, as it effected the rearrangement while simultaneously promoting methyl esterification and C3 deacetylation, delivering **18** in 90% yield. Subsequent epoxidation of the C12–C13 double bond furnished epoxide **19** (**Table S1**).

Mechanistic interrogation revealed that the outcome of this first rearrangement reflects a delicate interplay between kinetic and thermodynamic control. While the mono-migrated products **18a**/**18** are accessible under selected conditions,

they can undergo further transformation to the double-migrated product **18b** upon treatment with Lewis acids, indicating that **18b** represents the thermodynamically favored state. In this sense, the first migration is kinetically accessible, whereas the second migration becomes feasible once the initially formed carbocation can equilibrate to a more stable allylic cation manifold. Solvent effects are also critical: highly ionizing and protic solvents such as HFIP and MeOH likely alter the relative lifetimes and reactivity of the carbocation intermediates, enabling selective interception of mono-migrated products before full equilibration to the thermodynamic endpoint. Consistent with this interpretation, isolated **18a** was converted to **18b** upon treatment with BF_3•OEt_2. To further benchmark our system against Corey's precedent, we also examined the corresponding Corey substrate **17e**. Under BF_3•OEt_2, both the mono-migrated product **17f** and the double-migrated product **17i** were formed, whereas $Sc(OTf)_3$ delivered **17f** in 90% yield. As in the case of **18a**, isolated **17f** could be further converted into the thermodynamically more stable product **17i**. Reaction concentration also proved important: under Corey's highly dilute conditions (0.004 M), a more complex mixture was obtained, including **17f–h**, and comparison with authentic material allowed us to revise the structure previously assigned as **17j** to **17f**.

With the mono-migrated product **18** in hand, we next investigated the second methyl migration / cyclopropane-opening cascade through a Meinwald-initiated rearrangement (**Scheme 4**). Selective epoxidation of **18** with m-CPBA afforded epoxide **19**. Upon acid-promoted opening of the epoxide, we envisaged formation of carbocation intermediate **19a**, from which several competing pathways are accessible: alkyl migration to give the ring-contracted aldehyde **20a** (path a), hydride shift to give ketone **20b** (path b), methyl migration followed by deprotonation to give **20c** (path c), or a productive cascade involving sequential migration, cyclopropane opening, and carbocation trapping to furnish the desired oxygen-bridged product **20** (path d). A further cyclopropane-opening process of **20c** could also lead to **20d** (path e).

Systematic condition screening for this rearrangement (**Table 2**) revealed pronounced effects of both acid and solvent on product distribution. In DCM, both Brønsted acids (TFA, TsOH, PPTS) and Lewis acids (BF_3•OEt_2, Et_2AlCl) gave poor selectivity, affording mixtures of rearranged products. When HFIP was employed as solvent, several acids, including $Cu(OTf)_2$, $Zn(OTf)_2$, $CoCl_2$, and ionic liquids, predominantly furnished the hydride-shift product **20b**. Gratifyingly, the combination of PPTS/HFIP efficiently promoted the desired cascade, delivering **20** in 62% yield, and the structure of **20** was unambiguously confirmed by single-crystal X-ray diffraction. Re-entry experiments provided further mechanistic insight. Intermediate **20c** was converted cleanly into **20d** under TsOH or $Sc(OTf)_3$ in DCM, whereas **20c** failed to transform into **20** under PPTS/HFIP conditions. These results indicate that **20** is formed through a distinct productive reaction channel, rather than by secondary equilibration of **20c**. The full screening dataset (**Table S2**) likewise shows that hydride-shift product **20b** predominates under many conditions, indicating that hydride transfer is kinetically favored relative to the productive methyl-migration/ring-expansion sequence. For example, with TFA, BF_3•OEt_2, or HF (**entries 1–3**), four products were detected, including aldehyde **20a** and diol **20c**; Et_2AlCl or PPTS in conventional solvents (**entries 4–5**) failed to afford **20**; and TsOH (**entry 6**) gave **20d** as the major product (42% yield). Overall, these data indicate that the unique ability of HFIP to stabilize cationic intermediates while suppressing elimination and off-pathway rearrangements is critical for channeling the cascade toward formation of **20**.

Taken together, these results indicate that hydride migration is kinetically preferred, whereas methyl migration pathways require more stabilized carbocation environments. Importantly, re-entry experiments demonstrate that intermediates such as **20c** do not readily converge to **20** under optimized conditions, suggesting that formation of **20** proceeds through a distinct reaction channel rather than via equilibration from alternative products. More broadly, the outcome of these skeletal rearrangements is not dictated by a single intrinsic preference, but by a dynamic interplay between substrate structure, acid identity, and reaction medium, all of which reshape the relative accessibility of competing pathways.

3) DFT Calculations and Mechanistic Analysis

To elucidate the origin of selectivity in both the lactone-initiated dyotropic rearrangement and the subsequent Meinwald cascade, preliminary DFT calculations were carried out at the SMD(MeOH/HFIP)-M06-2X-D3/def2-TZVPP//B3LYP-D3(BJ)/def2-SVP level of theory (full computational details are provided in the Supporting Information), and the resulting Gibbs free energy profiles are shown in **Scheme 6**. For the initial Wagner- Meerwein rearrangement, the calculations indicate that the first C13 methyl migration from protonated lactone precursor **17a** proceeds via dyotropic rearrangement transition state TS-1 with a barrier of $\Delta G^{\ddagger}$ = 7.65 kcal mol^{-1}, furnishing protonated lactone intermediate **17b**. From **17b**, deprotonation at C12 gives the mono-migrated alkene **18a**, whereas deprotonation at the lactone moiety furnishes **18c**.

In contrast, the subsequent C14 methyl migration occurs via TS-2 with a substantially higher barrier of [$\Delta G^{\ddagger}$ = 16.49 kcal mol^{-1}] and ultimately leads, after hydride shifts, cyclopropane opening, and alkene isomerization, to the thermodynamically more stable diene product **18b**, which lies [ΔG = –5.56 kcal mol^{-1}] below **18a**. These results are consistent with the experimental observation that mono-migrated products (**18a/18**) can be formed under kinetically controlled conditions, whereas further rearrangement to the double-migrated product **18b** becomes accessible under conditions that allow carbocation equilibration. In this sense, the first migration is kinetically accessible, whereas progression to **18b** is thermodynamically favored **(Figure S1)**.

The calculations also support the experimentally observed interconversion behavior. Because **18b** is significantly lower in energy than **18a**, it can be regarded as the thermodynamic sink of this rearrangement manifold, whereas **18a/18** represent kinetically trapped products. This interpretation is fully consistent with the re-entry experiment in which isolated **18a** is converted to **18b** upon treatment with **BF_3•OEt_2.** Similarly, Corey's mono-migrated substrate **17f** could also be converted to the corresponding thermodynamically more stable diene **17i**, further supporting the same mechanistic picture.

For the Meinwald rearrangement cascade, several pathways from epoxide-derived carbocation **19a** were evaluated, including hydride shift, methyl migration, alkyl migration, and cyclopropane opening. The calculations indicate that the hydride-shift pathway leading to **20b** is kinetically highly competitive and accounts for the experimentally observed predominance of **20b** under many conditions. By contrast, formation of the desired oxygen-bridged product **20** requires a more elaborate sequence involving C14 methyl migration, subsequent hydride shift, and cyclopropane opening through TS-7, TS-9, and TS-10, with a highest barrier of $\Delta G^{\ddagger}$ = 16.08 kcal mol^{-1}. These results explain why the productive pathway is observed only under carefully optimized conditions and why multiple side products are readily formed **(Figure S2)**.

The calculations further clarify the relationship between **20** and **20d**. Although both products arise from the cyclopropane-opening manifold, they diverge from intermediate **19**. Product **20d** is calculated to be thermodynamically more stable than **20** by 7.93 kcal mol^{-1}, whereas formation of **20** is kinetically favored. Specifically, the largest barrier along the productive pathway from **19** to **20** is 11.85 kcal mol^{-1}, whereas conversion of **20c** to **20d** proceeds through a higher barrier of 16.08 kcal mol^{-1}. This interpretation is consistent with the experimental findings that **20c** is converted to **20d** under acidic conditions in DCM, but does not converge to **20** under PPTS/HFIP conditions. Thus, **20** does not arise from secondary equilibration of **20c**, but instead from a distinct productive cascade.

Overall, the computational results support a model in which product distribution is governed by a delicate interplay between kinetic accessibility and thermodynamic stability of carbocationic intermediates, modulated by substrate structure, solvent, and acid environment. Taken together, the combined experimental and computational studies reveal a key feature of this system: carbocation-driven skeletal rearrangements are not dictated by a single intrinsic preference, but instead by a dynamic balance among migration propensity, cation stability, and termination mode. In the dyotropic rearrangement sequence, mono-methyl migration is kinetically accessible, whereas the more extensively rearranged diene **18b** corresponds to the thermodynamic endpoint. In the Meinwald cascade, the oxygen-bridged product **20** is

formed through a kinetically favored productive channel, whereas **20d** is thermodynamically more stable and therefore represents a lower-energy endpoint of the competing cyclopropane-opening manifold.

These findings also inform the biosynthetic discussion. Although the present 12,13-epoxide pathway is not intended as a literal proposal for the enzymatic sequence operating in vivo, it captures the key skeletal logic required to transform a cycloartane precursor into the glycinoeclepin framework. In this sense, the present work is best viewed as a bioinspired chemical emulation of plausible skeletal reorganization pathways, rather than as a definitive biomimetic reconstruction of glycinoeclepin biosynthesis.

4) Late-stage oxidations and photo-oxidative decarbonylation to glycinoeclepin A

With the key carbon framework in place, we next turned to the late-stage oxidative manipulations required for selective B-ring decarbonylation. After protection of C12–OH as the acetate, the C14–C15 alkene was installed through SeO_2-mediated allylic oxidation followed by elimination. Direct C7 allylic oxidation proved nontrivial: a range of standard conditions, including CrO_3/3,5-DMP[35], PDC/*t*-BuOOH[36], Pd/C/*t*-BuOOH[37], CuI/*t*-BuOOH[38], $Rh(cap)_4$/*t*-BuOOH[39], and $Mn(OAc)_3$/*t*-BuOOH[40], led either to substrate decomposition or competitive oxidation at C16. In contrast, treatment with SeO_2/pyridine cleanly furnished the C7 hydroxylated product, which was subsequently oxidized to ketone **22**.

We then addressed installation of the C6 hydroxyl group via α-oxidation of the adjacent ketone. Several commonly used protocols, including Davis oxidation[41], LiHMDS/O_2/$P(OEt)_3$, and *t*-BuOK/O_2, proved ineffective, and Corey's conditions also failed, most likely owing to steric congestion around C12. Ultimately, a sequence consisting of enol silylation (LDA/TMSCl), Rubottom oxidation[42] with *m*-CPBA, and desilylation provided the desired α-hydroxy product. Further oxidation at C6 required careful tuning: DMP, TEMPO, and Swern conditions predominantly promoted undesired C6–C7 bond cleavage, whereas mild $Cu(OAc)_2$/MeOH[43] delivered **23** in satisfactory yield with useful chemoselectivity.

With these functionalities in place, we turned to selective cleavage of the B ring. Periodate failed to effect the desired C–C bond scission. Gratifyingly, adoption of Takeda's photo-oxidative protocol[44] (methylene blue, O_2, tungsten-lamp irradiation) afforded **24** in high yield. This transformation is consistent with a mechanism in which photo-generated singlet oxygen undergoes an intramolecular oxygen-*ene* reaction to form a five-membered endoperoxide intermediate (**23b**), followed by O–O homolysis and extrusion of CO to achieve decarbonylation. Finally, one-pot hydrolysis of both the acetate and methyl ester with LiOH furnished glycinoeclepin A (**1**). The structure of **23** was confirmed by single-crystal X-ray diffraction, and the spectroscopic data and optical rotation of synthetic **1** matched those reported by Mori, thereby validating our structural assignments.

Notably, both the Meinwald-type cascade and the photo-oxidative decarbonylation proceed under relatively mild, nature-compatible conditions (H^+; O_2/hv), suggesting that analogous transformations could be chemically feasible in a biosynthetic setting. Although we do not claim that the present sequence directly reproduces the enzymatic pathway operating in vivo, the isolation and characterization of **19** and **23** as discrete intermediates provide experimentally testable support for the proposed skeletal logic and offer potential chemical markers for targeted metabolomic studies in legumes or associated microbiota. In this sense, the present route not only enables chemical access to glycinoeclepin A, but also serves as a bioinspired platform for interrogating plausible rearrangement manifolds in eclepin-type biogenesis and for guiding the discovery of as-yet-unidentified members of this family.[45-47]

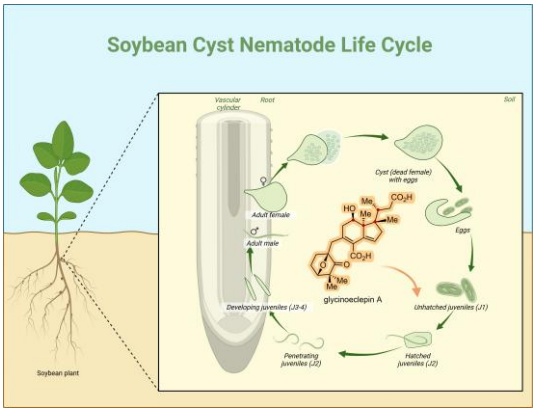
Conclusion

In summary, we have established a bioinspired route to glycinoeclepin A (**1**) in 17 steps from aldehyde **15**, itself derived from readily available γ-oryzanol, with an overall yield of 2%. A directed C–H oxidation enables site-selective C17 functionalization together with concomitant C23–C24 scission, thereby providing decagram-scale access to a

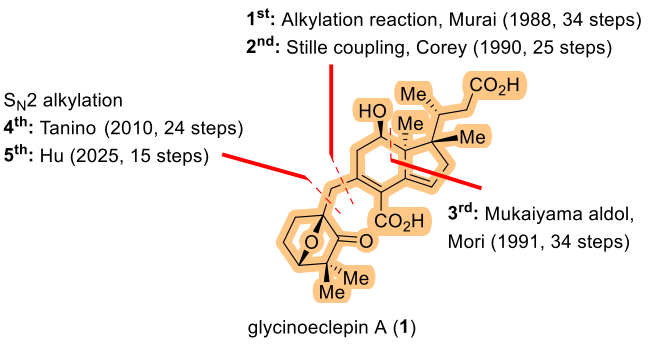
pivotal lactone intermediate. A programmed skeletal reorganization, comprising a dyotropic rearrangement followed by epoxidation and a Meinwald cascade, assembles the oxygen-bridged A/B framework, installs the C12 stereogenic hydroxyl group, and establishes the quaternary centers at C13 and C17 with high stereocontrol. A late-stage photo-oxidative decarbonylation then selectively excises the C6 carbonyl within the B ring to furnish the natural product.

Beyond providing practical and scalable access to glycinoeclepin A (**1**), this work offers mechanistic insight into carbocation-driven skeletal rearrangements and demonstrates how subtle changes in substrate structure and reaction environment can profoundly alter reaction pathways. More broadly, these findings provide a chemically grounded framework for evaluating related biosynthetic hypotheses and suggest new opportunities for late-stage skeletal editing and biogenetically inspired design in complex triterpenoid synthesis.

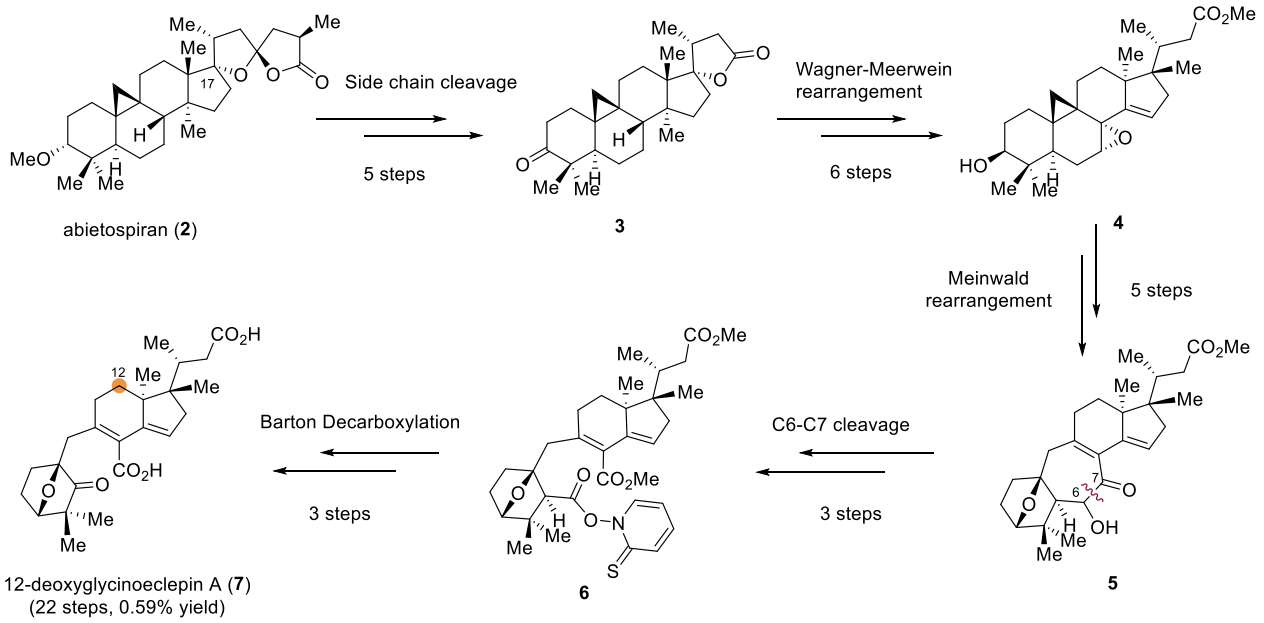
a. Soybean cyst nematode life cycle and glycinoeclepin A (**1**)



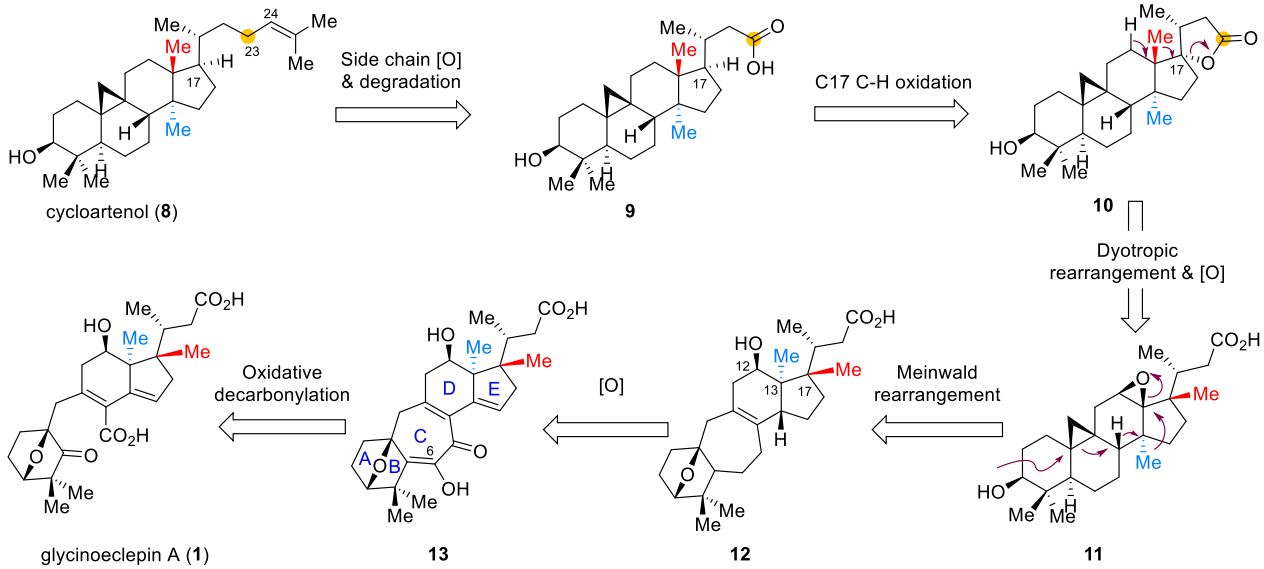
b. Total synthesis of glycinoeclepin A (**1**)



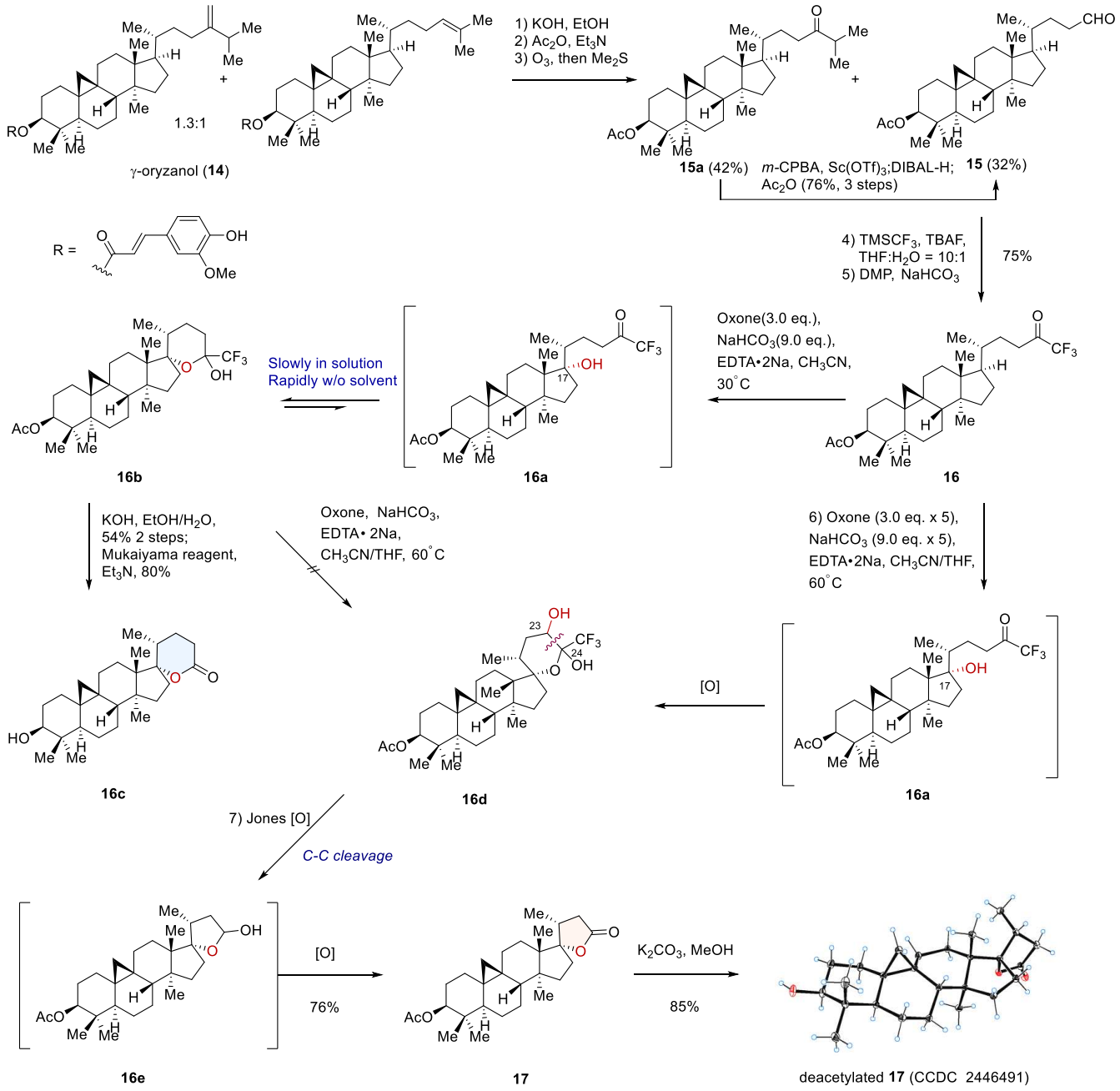
c. Corey's biomimetic synthesis of 12-deoxyglycinoeclepin A (**7**)



d. Synthetic design of glycinoeclepin A (**1**) based on biosynthetic network analysis (This work)

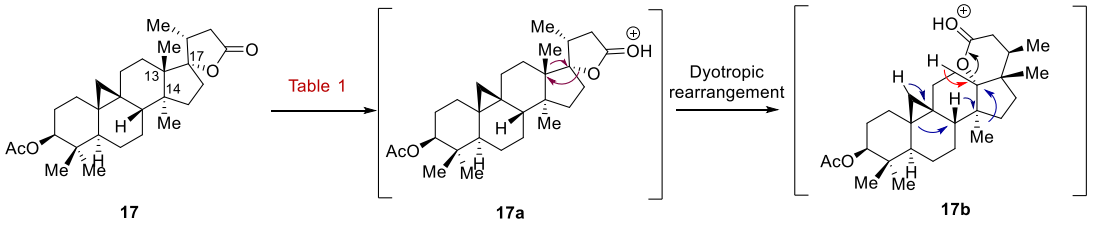


Scheme 1. Soybean cyst nematode and synthetic progress of glycineclepin A (**1**).

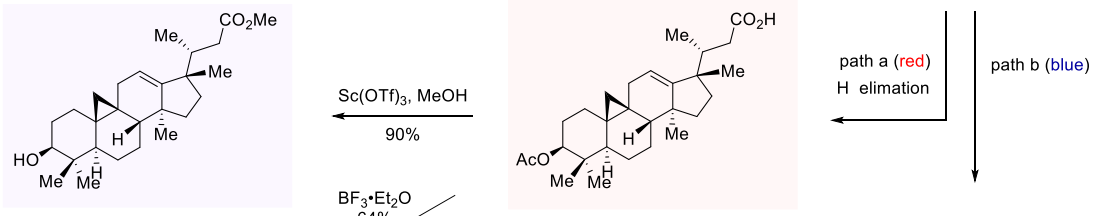


Scheme 2. C-17 sp^3 C-H bond hydroxydation.

a. Wagner-Meerwein rearrangement



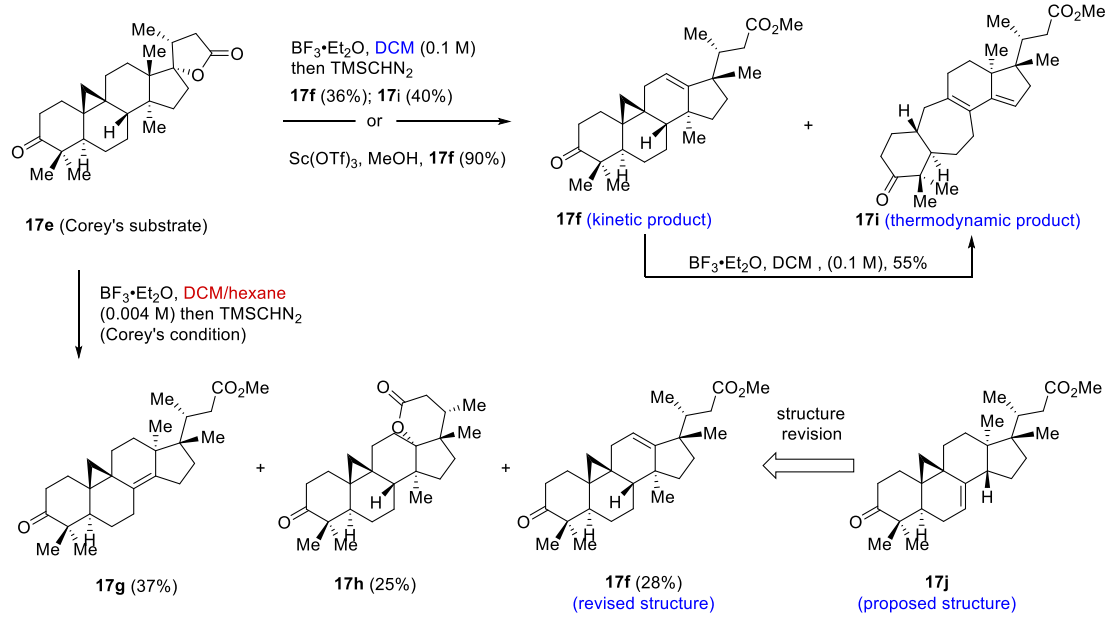
17 **17a** **17b**



18 (desired, kinetic product) **18a**

18b (undesired, thermodynamic product) **17d** **17c**

b. Control experiments

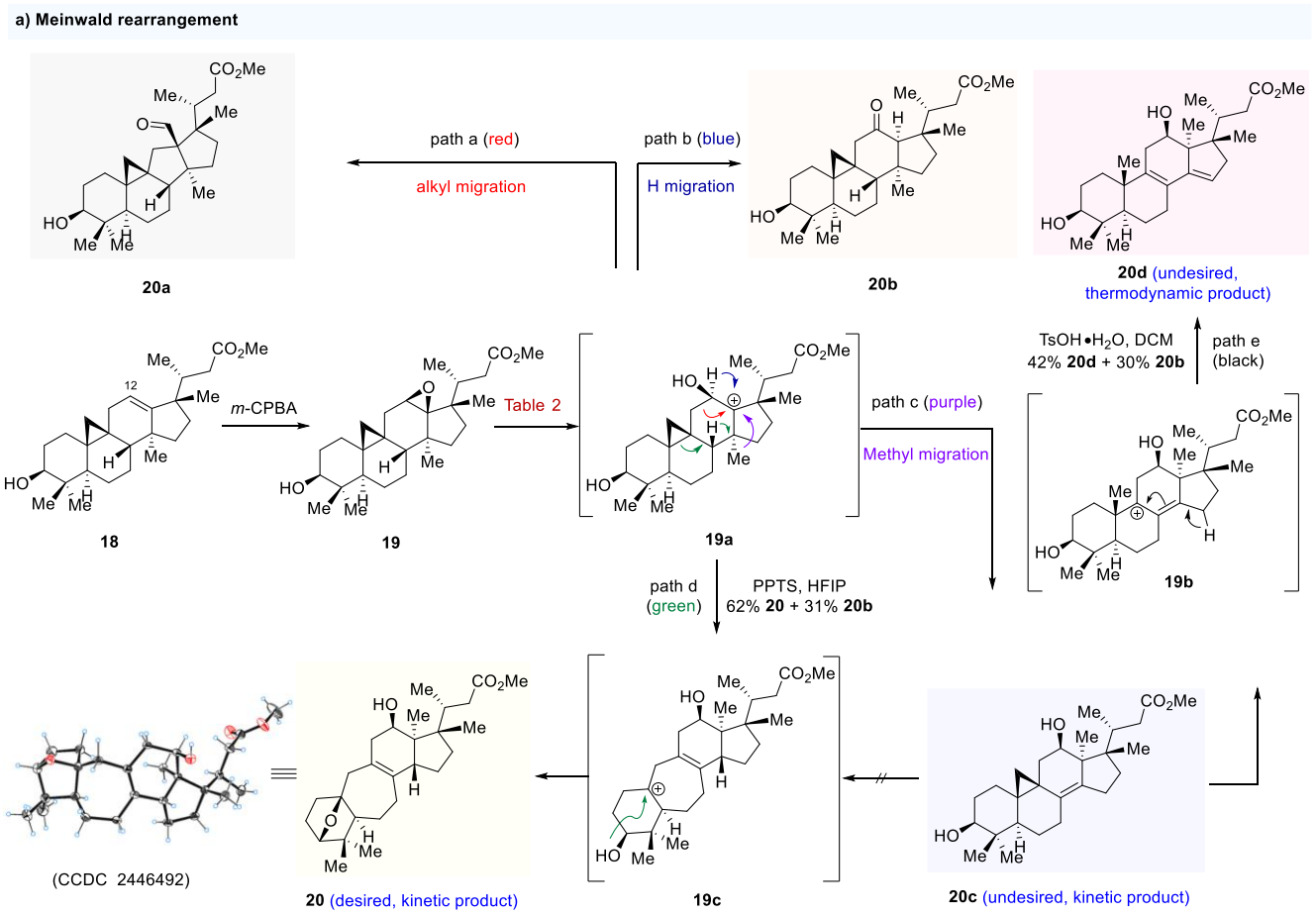


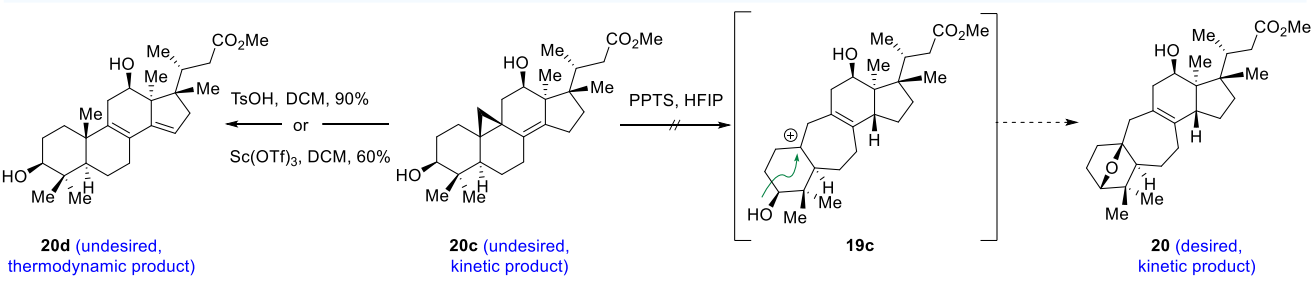
17e (Corey's substrate)

17f (kinetic product) **17i** (thermodynamic product)

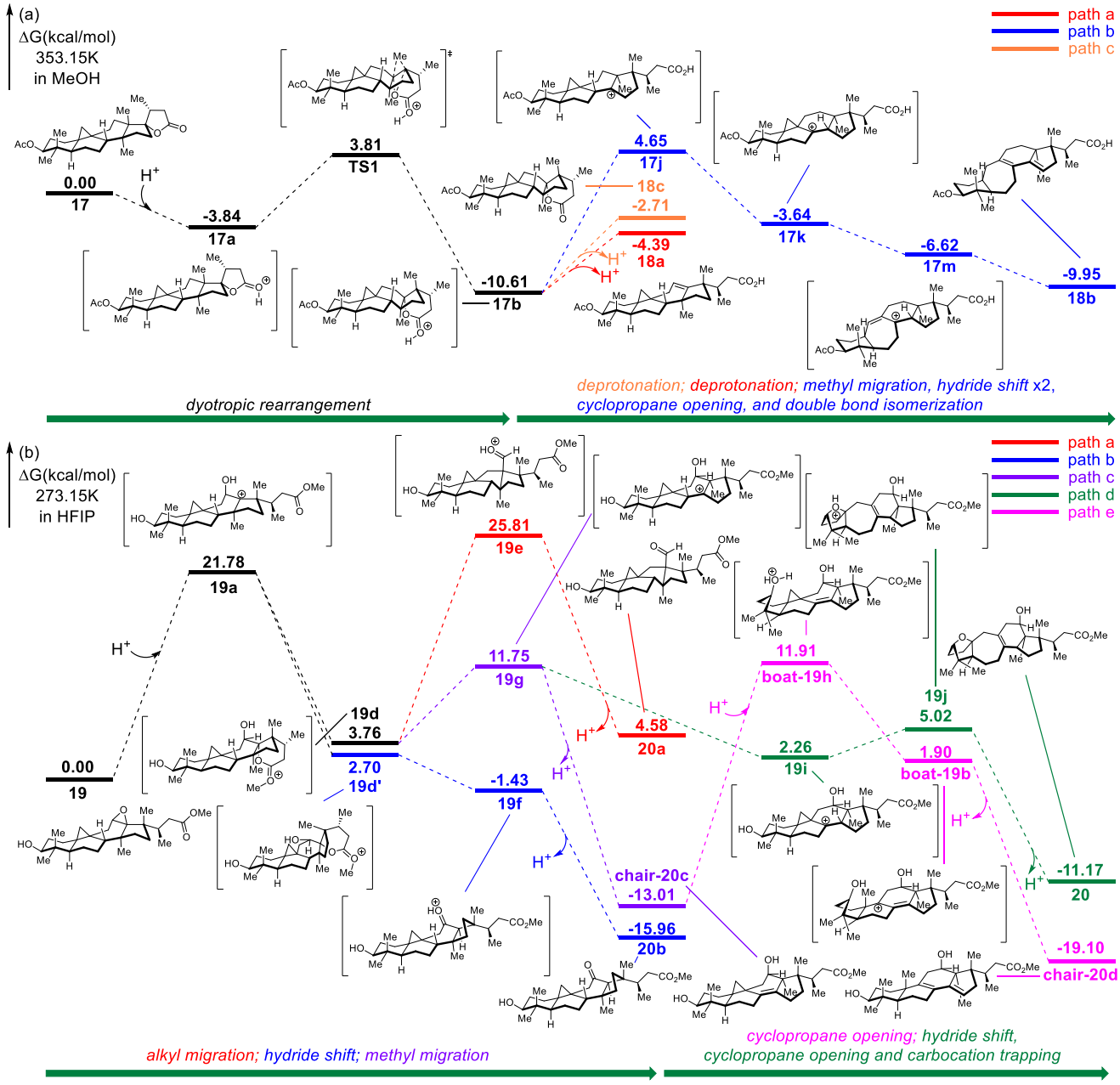
17g (37%) **17h** (25%) **17f** (28%) (revised structure) **17j** (proposed structure)

Scheme 3. Synthesis of **18** through dyotropic rearrangement.

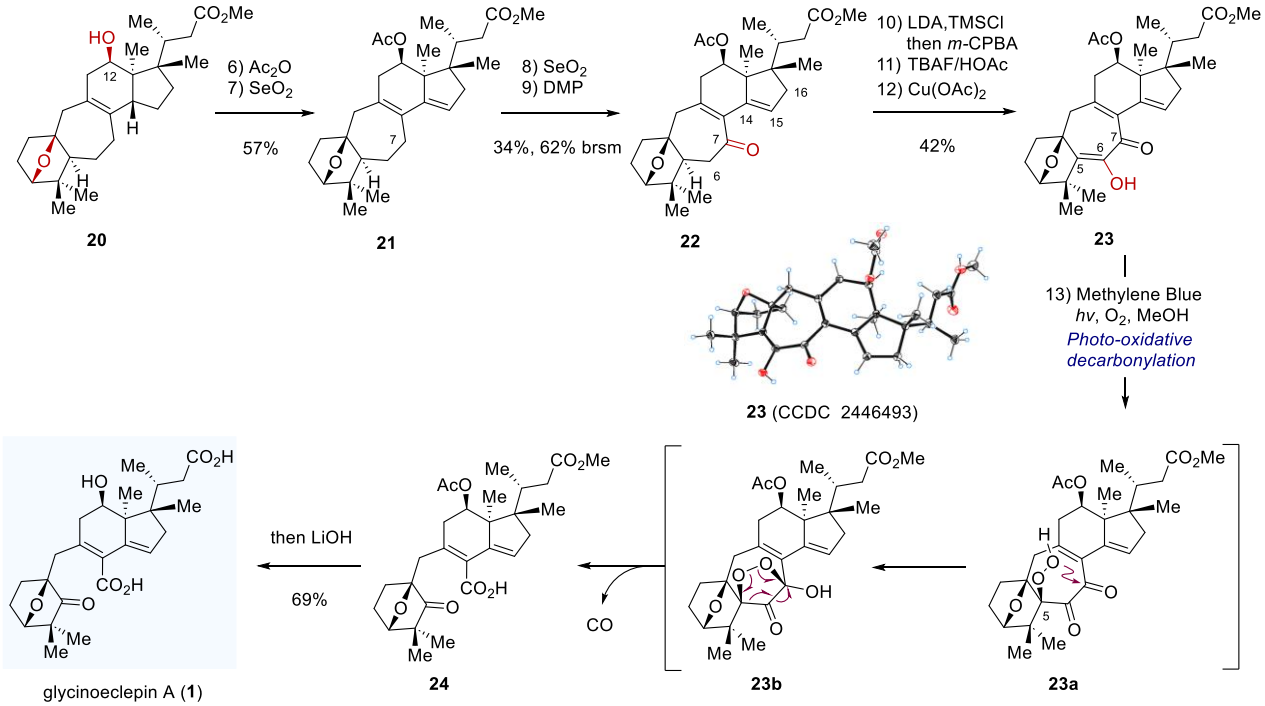




Scheme 4. Synthesis of **20** through Meinwald rearrangement.



Scheme 5. DFT-computed free-energy profiles for competing carbocation rearrangement pathways.



Scheme 6. Synthesis of glycineclepin A (**1**).

Table 1. Optimization of dyotropic rearrangement.

Entry	Conditions[a]	Product (yield)
1	TFA, DCM, 15℃.	NR
2	Et_2AlCl, DCM, 15℃.	NR
3	$FeCl_3$, DCM, 15℃.	**18a** (32%), **18b** (41%)
4	BF_3•OEt_2, DCM, 15℃.	**18a** (43%), **18b** (39%)
5	$Bi(OTf)_3$, DCM, 15℃.	**18a** (60%)
6	$Sc(OTf)_3$, DCM, 15℃.	**18b** (42%)
7	$Sc(OTf)_3$, HFIP, 0℃	**18b** (60%)
8	TFA, HFIP, 0℃	Mess
9	$Bi(OTf)_3$, HFIP, 0℃	**18b** (42%)
10	TsOH, HFIP, 0℃	**18b** (46%)
11	$Sc(OTf)_3$[b], MeOH, 80℃	**18** (90%)
12	$Bi(OTf)_3$, MeOH, 80℃	**18** (81%)
13	$FeCl_3$, MeOH, 80℃	Mess
14	H_2SO_4 (2.0 M in dioxane), 80℃	Deacetylation-**18a** (80%)

[a] 1.0 equiv.; [b] 2.0 equiv.

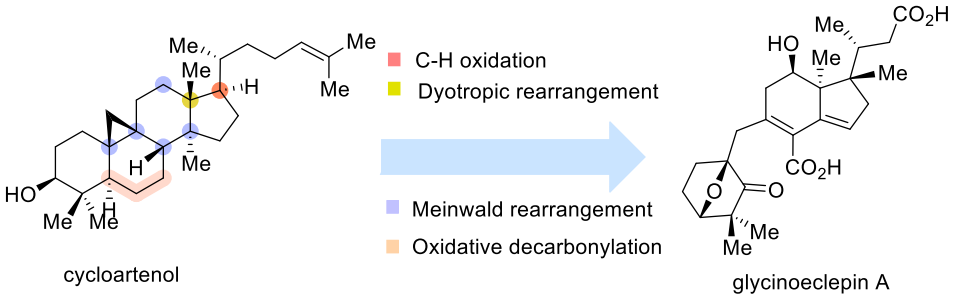
Table 2. Optimization of Meinwald rearrangement.

Entry	Conditions[a]	Product (yield)

1	TFA, DCM, 0℃	**20** (8%), **20a** (9%), **20b** (38%), **20c** (34%)
2	BF_3•OEt_2, DCM, –50℃	**20** (32%), **20a** (7%), **20b** (41%), **20c** (6%)
3	HF, CH_3CN/DCM, 0℃	**20** (41%), **20a** (4%), **20b** (37%), **20c** (8%)
4	Et_2AlCl, DCM, –50℃	**20** (48%), **20a** (17%), **20c** (24 %)
5	PPTS, DCM, 25℃	**20b** (35%), **20a** (10%), **20c** (44 %)
6	TsOH, DCM, 0℃	**20** (5%), **20a** (6%), **20b** (30%), **20d** (42%)
7	$Sc(OTf)_3$, DCM, 0℃	**20** (45%), **20a** (10%), **20b** (33%)
8	$[EMIM]BF_4$, HFIP, 0℃	**20** (29%), **20b** (58%)
9	$Zn(OTf)_2$, HFIP, 0℃	**20** (24%), **20b** (63%)
10	$Cu(OTf)_2$, HFIP, 0℃	**20b** (87%)
11	$CoCl_2$, HFIP, 0℃	**20** (41%), **20b** (45%)
12	PPTS, HFIP, 0℃	**20** (62%), **20b** (31%)

[a]1.0 equiv.

Table of Contents



cycloartenol

glycinoeclepin A

A bioinspired synthesis of glycinoeclepin A enables scalable access to a potent soybean cyst nematode hatching stimulus and provides mechanistic insight into carbocation-driven skeletal rearrangements.

Acknowledgements

Financial supported from the National Natural Science Foundation of China (nos. 22371142, 22571165, 22301146), Frontiers Science Center for New Organic Matter, Nankai University (no. 63181206), Key project at central government level: The ability establishment of sustainable use for valuable Chinese medicine resources (no. 2060302), the Fundamental Research Funds for the Central Universities (no. 23JCYBJC01410), Tianjin Major Science and Technology Project for National Key Laboratories (25ZXZSSS00370), Science Fund for

Distinguished Young Scholars of Tianjin Municipality (25JCJQJC00350) and China Postdoctoral Science Foundation (no. 332608) are gratefully acknowledged.

Keywords: Glycinoeclepin A • skeletal reorganization • bioinspired synthesis • biosynthesis • triterpenoids

References:

[1] A. Y. Bandara, D. K. Weerasooriya, C. A. Bradley, T. W. Allen, P. D. Esker, *PLoS ONE* **2020**, *15*, e0231141.

[2] K. Acharya, G. Yan, A. Plaisance, *Plant Dis.* **2021**, *105*, 764−769.

[3] N. Nissan, B. Mimee, E. R. Cober, A. Golshani, M. Smith, B. A. Samanfar, *Biology.* **2022**, *11*, 211.

[4] J. Ochola, D. Coyne, L. Cortada, S. Haukeland, M. Ng'ang'a, A. Hassanali, C. Opperman, B. Torto, *Pest Manag. Sci.* **2021**, *77*, 1150–1159.

[5] W. Chen, D. Wang, S. Ke, Y. Cao, W. Xiang, X. Guo, Q. Yang, *Nat. Microbiol.* **2024**, *9*, 1993–2005.

[6] Y. Arjoune, N. Sugunaraj, S. Peri, S. V. Nair, A. Skurdal, P. Ranganathan, B. Johnson, *Plant Methods* **2022**, *18*, 110.

[7] P. Yates, J. Janiol, C. Li, B. H. Song, *Plants* **2024**, *13*, 319.

[8] T. Masamune, M. Anetai, M. Takasugi, N. Katsui, *Nature* **1982**, *297*, 495–496.

[9] D. Ma, J. Ao, N. Hu, G. Liang, *Chin. J. Org. Chem.* **2021**, *41*, 553–566.

[10] A. Fukuzawa, A. Furusaki, M. Ikura, T. Masamune, *J. Chem. Soc. Chem. Commun.* **1985**, *4*, 222–224.

[11] A. Murai, N. Tanimoto, N. Sakamoto, T Masamune, *J. Am. Chem. Soc*. **1988**, *110*, 1985–1986.

[12] E. J. Corey, I. N. Houpis, *J. Am. Chem. Soc.* **1990**, *112*, 8997–8998.

[13] H. Watanabe, K. Mori, *J. Chem. Soc., Perkin Trans*. 1 **1991**, 2919–2934.

[14] Y. Shiina, Y. Tomata, M. Miyashita, K. Tanino, *Chem. Lett.* **2010***, 39*, 835–837.

[15] K. Shen, Q. Wang, T. Zhu, Y. Qiao, P. Hu, *J. Am. Chem. Soc.* **2025**, *147*, 23411–23416.

[16] E. J. Corey, B. C. Hong, *J. Am. Chem. Soc.* **1994***, 116*, 3149–3150.

[17] P. Ellerbrock, N. Armanino, M. K. Ilg, R. Webster, D. Trauner, *Nat. Chem*. **2015**, *7*, 879–882.

[18] (a) K. Shimizu, R. Akiyama, Y. Okamura, C. Ogawa, Y. Masuda, I. Sakata, B. Watanabe, Y. Sugimoto, A. Kushida, K. Tanino, M. Mizutani, *Sci. Adv*. **2023**, *9*, eadf4166. (b) A. Eschenmoser, D. Arigoni, *Helv. Chim. Acta* **2005**, *88*, 3011-3050.

[19] (a) X. Long, H. Wu, Y. Ding, C. Qu, J. Deng, *Chem* **2021**, *7*, 212–223. (b) S. Hua, W, Zhong, L, Chen, Y. Jia, Nat.*Commun.* **2026**, 10.1038/s41467-026-71602-w. (c) S. Seong, H. Lim, S. Han, *Chem* **2019**, 5, 353–363.

[20] N. Y. Lam, K. Wu, J. Q. Yu, *Angew. Chem. Int. Ed.*, **2021**, *60*, 15767–15790.

[21] T. Dalton, T. Faber, F. Glorius, *ACS Cent. Sci.* **2021**, *7*, 245–261.

[22] J. H. Docherty, T. M. Lister, G. Mcarthur, M. T. Findlay, P. Domingo-Legarda, J. Kenyon, S. Choudhary, I. Larrosa, *Chem. Rev.* **2023**, *123*, 7692–7760.

[23] I. Bakanas, R. F. Lusi, S. Wiesler, J. Hayward Cooke, R. Sarpong, *Nat. Rev. Chem.* **2023**, **7**, 783–799.

[24] P. Tao, Y. Jia, *Sci. China Chem.* **2016**, *59*, 1109–1125.

[25] H. Renata, *Chem. Soc. Rev.* **2025**, *54*, 7913–7932.

[26] (a) M. Alekseychuk, S. Adrian, R. C. Heinze, P. Heretsch, *J. Am. Chem. Soc.* **2022**, *144*, 11574–11579. (b) X. Long, J. Li, F. Gao, H. Wu, J. Deng, *J. Am. Chem. Soc*. **2022**, *144*, 16292–16297. (c) M. Kizakis, M. Treger, G. Dräger, C. König, P. Heretsch, *J. Am. Chem. Soc.* **2026***, 148,* 13912-13920.

[27] D. Yang, M. K. Wong, X. C. Wang, Y. C. Tang, *J. Am. Chem. Soc.* **1998**, *120*, 6611–6612.

[28] G. K. S. Prakash, R. Krishnamurti, G. A. Olah, *J. Am. Chem. Soc.* **1989***, 111*, 393–395.

[29] G. Lesma, A. Luraghi, T. Bavaro, R. Bortolozzi. G. Rainoldi, G. Roda, G. Viola, D. Ubiali, A. Silvani, *J. Nat. Prod.* **2018**, *81*, 2212–2221.

[30] J. Jurczyk, J. Woo, S. F. Kim, B. D. Dherange, R. Sarpong, M. D. Levin, *Nat. Synth*. **2022**, *1*, 352–364.

[31] S. F. Kim, C. Amber, G. L. Bartholomew, R. Sarpong, *Acc. Chem. Res*. **2025**, *58*, 1786–1800.

[32] R. Al-Ahmad, M. Dai, *Acc. Chem. Res.* **2025**, *58*, 1392–1406.

[33] Z. Zhang, X. Qian, Y. Gu, J. Gui, *Nat. Prod. Rep.* **2024**, *41*, 251–272.

[34] For recent examples of dyotropic rearrangement, see: (a) C. Hugelshofer, T. Magauer, *Nat. Prod. Rep.*, **2017**, *34*, 228–234. (b) J. Cao, H. Wu, Q. Wang, J. Zhu, *Nat. Chem.* **2021**, *13*, 671–676. (c) Y. Li, J. Zhang, Y. Chen, J. Pang, Y. Chen, Y. Tang, *Angew. Chem. Int. Ed.* **2025**, *64*, e202414985. (d) Y. Niu, Y. Chen, M. Zhou, H. Zeng, K. Wang, P. Yu, Z. Dong, *Science* **2026**, *391*, 171–178.

[35] W. G. Salmond, M. A. Barta, *J. Org. Chem.* **1978**, *43*, 2057–2059.

[36] N. Chidambaram, S. Chandrasekaran, *J. Org. Chem*. **1987**, *52*, 5048–5051.

[37] J. Q. Yu, E. J. Corey, *Org. Lett.* **2002**, *4*, 2727–2730.

[38] J. A. R. Salvador, M. L. S. Melo, A. S. C. Neves, *Tetrahedron Lett*. **1997**, *38*, 119–122.

[39] A. J. Catino, R. E. Forslund, M. P. Doyle, *J. Am. Chem. Soc.* **2004**, *126,* 13622–13623.

[40] T. K. Shing, Y. Y. Yeung, P. -L. Su, *Org. Lett.* **2006**, *8*, 3149–3151.

[41] F. A. Davis, L. C. Vishwakarma, J. G. Billmers, *J. Org. Chem.* **1984**, *49*, 3241–3243.

[42] G. M. Rubottom, M. A. Vazquez, D. R. Pelegrina, *Tetrahedron Lett*. **1974**, *15*, 4319–4322.

[43] N. L. Wendler, D. Taub, R. P. Graber, *Tetrahedron* **1959**, *7*, 173–184.

[44] M. Utaka, M. Nakatani, A. Takeda, *Tetrahedron Lett*. **1983**, *24*, 803–806.

[45] M. Razzak, J. De Brabander, *Nat. Chem. Biol.* **2011***, 7*, 865–875.

[46] B. E. Hetzler, D. Trauner, A. L. Lawrence, *Nat. Rev. Chem.* **2022**, *6*, 170–181.

[47] A. J. Novak, C. E. Grigglestone, D. A. Trauner, *J. Am. Chem. Soc.* **2019**, *141*, 15515–15518.

[48] Deposition numbers 2446491 (for **17**), 2446492 (for **20**), and 2446493 (for **23**) contain the supplementary crystallographic data for this paper. These data are provided free of charge by the joint Cambridge Crystallographic Data Centre and Fachinformationszentrum Karlsruhe Access Structures service.

Supplementary Files

This is a list of supplementary files associated with this preprint. Click to download.

- SupportingInformation.pdf